Ying-Chu Chen (Autor)

Advanced Nanoarchitectures with Photocatalytic Functionality

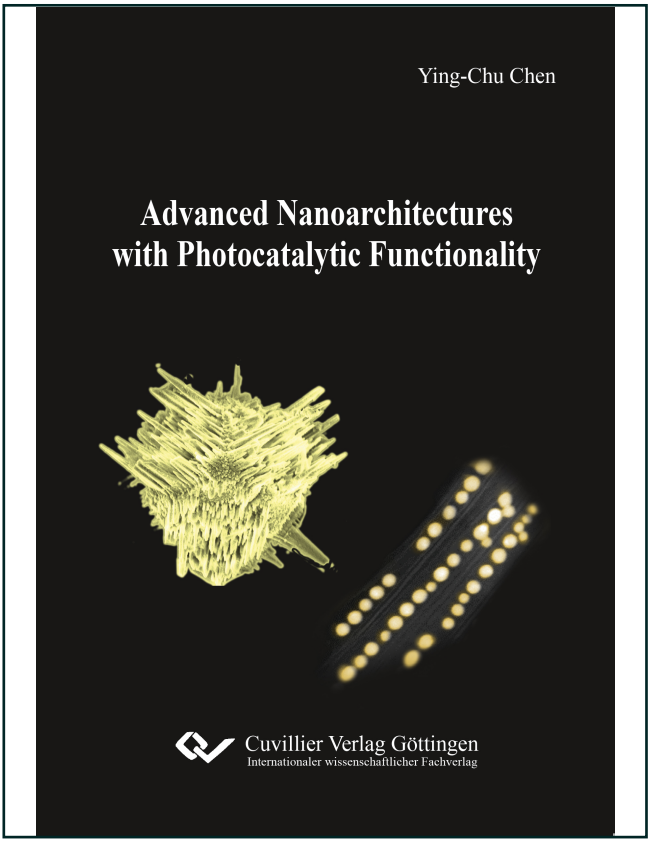

https://cuvillier.de/de/shop/publications/7792

1. Introduction and Brief History

Nature is the starting point for advancing science and technology. Replication and adaption of natural systems including elements, structures and processes, so-called biomimicry, routinely help humans to solve problems throughout their existence.[1] One of the extensively studied themes in this field is the photosynthesis in plants. The featured solar-to-chemical energy conversion involved in this course has triggered worldwide scientists and engineers to emulate using man-made materials. This is generally called artificial photosynthesis. The first demonstration was performed in 1839 by Becquerel.[2] In his study, the charge transfer involved in a sunlight-driven chemical reaction was manifested in an electric current flowing from an illuminated silver chloride electrode immersed in an acidic chemical medium to a metallic counter electrode *via* an external circuit (Fig. 1.1). Extensive studies followed up his unprecedented work with a systematic investigation on such photoelectrochemical phenomena in other semiconducting materials, such as Si, Ge, GaAs, ZnO, CdSe, $KTaO_3$, $SrTiO_3$ and TiO_2.[3-28] These pioneering works prior to 1970 substantially established the fundamentals of photoelectrochemistry. Afterwards, the work by Fujishima and Honda in 1972 was of particular importance.[29] They used TiO_2 as the electrode material, which was irradiated under a photoflux to split water (H_2O) and which is similar in many respects to natural photosynthesis. The significance of their results lies in reinforcing the availability of oxygen (O_2) and especially of hydrogen (H_2), which is the next-generation clean fuel, upon water cleavage under renewable sunlight casting. More importantly, the sustainability and environmental benignity in the context of this photoelectrosynthesis effectively alleviate contemporary public concerns with the oncoming exhaustion of fossil fuel and global temperature increases.

Although the solar fuel generation is of primary importance, other nowadays critical issues in addition to the global warming including food crisis and water stress can also be mitigated *via* artificial photosynthesis. In particular, the reduction of primary greenhouse gas carbon dioxide (CO_2) to carbohydrates,[30] the production of ammonium (NH_4^+) and nitrate (NO_3^-) fertilizers from atmospheric nitrogen (N_2)[31] and the remediation of raw and waste water[32] are all possible *via* photoelectrocatalysis, thus stimulating a tremendous research activity in this realm. Further important early contributions emerged between 1978 and 1979 by Bard,[33] who established the principles of photoelectrocatalysis (PEC) not only applicable to a cell configuration but also appropriate for a particulate system (miniaturized metallic counter electrode granulates the semiconductor colloids), and by Nozik,[34] who formulated such concept of a short-circuited photoelectrocatalytic cell as a “photochemical diode”.

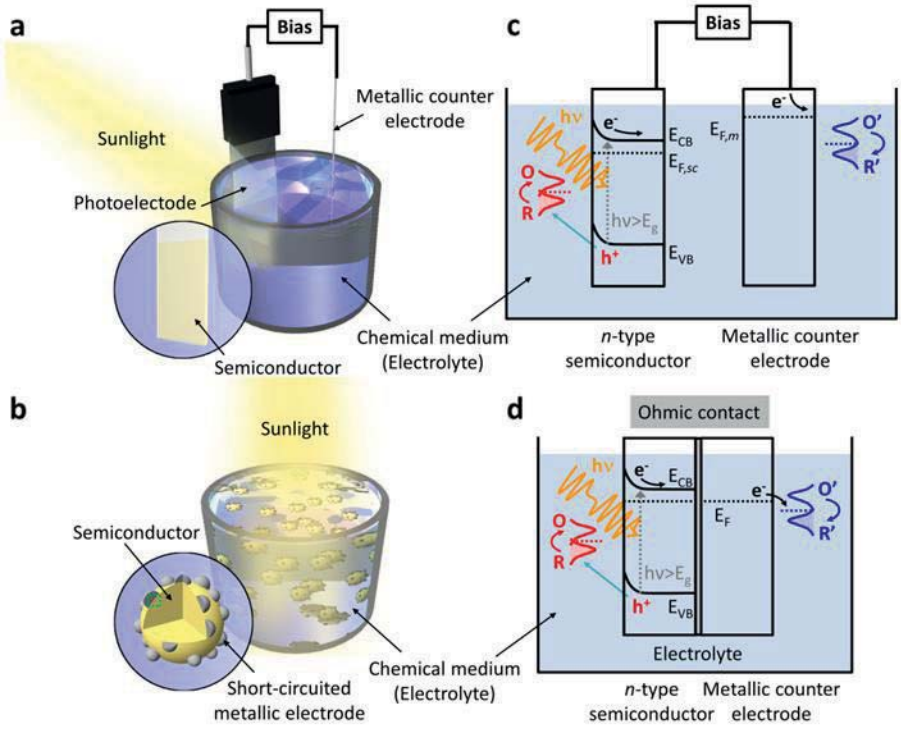

Figure 1. 1. (a) Electrochemical cell and (b) suspended metallized powder configurations for carrying out photoelectrocatalysis using *n-type* semiconductor. Energetics of the (c) photoelectrochemical cell and (d) photochemical diode (framed region in Fig. 1.1b). Abbreviations used: $h\nu$, photon energy; E_g, bandgap of the semiconductor; E_{CB}, conduction band edge of the semiconductor; E_{VB}, valence band edge of the semiconductor; $E_{F,sc}$, Fermi level of the semiconductor; $E_{F,m}$, Fermi level of the metallic counter electrode; E_F, Fermi level of the metallized semiconductor.

Their formulations advanced the development in many aspects, including i) the material scope branching out into semiconductors having high electrical resistivity that cannot work as an electrode, ii) the synthetic field opened up to additional more facile but less expensive protocols, and iii) the efficiency record of solar-to-chemical conversion going up to a new plateau owing to strong light scattering within the suspended particles (Fig. 1.2). Later in the early eighties, Grätzel's group excellently exemplified their argumentation with a series of experimental evidences using a variety of semiconducting colloids.[35-37] More importantly, most colloids were characterized by a particle size of few tens of nanometers, rendering these reports acknowledged as another significant milestone highlighting the fusion of modern nanoscience with photoelectrochemistry. The use of nanomaterials in the *bias-free* photochemical diode brings numerous advantages, including shortening the migration pathway of photogenerated carriers (electrons (e^-) and holes (h^+)) within semiconducting materials and increasing the surface area for carrier transfer across the solid/liquid

interface.[33,34] Most significantly, the specific size quantization effect renders the optoelectronic properties, e.g. the bandgap, the carriers' lifetime and the catalytic activity of these nanoscale granules, size-adaptable.[38-40]

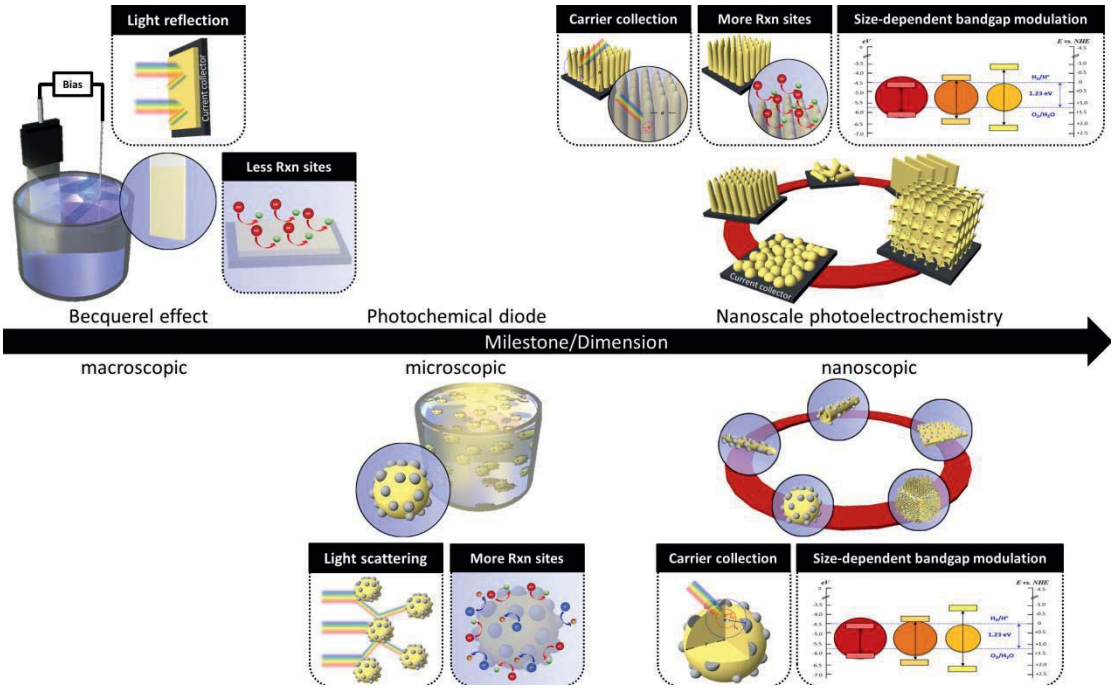

Figure 1. 2. Chronological summary of significant milestones, including dimensional migration and nanostructuring strategies, in photoelectrochemistry. Abbreviations used: L_h, mean free diffusion length of the hole (h^+); L_e, mean free diffusion length of the electron (e^-). Geometries of the exemplary nanoparticle and nanotip are characterized by the radius (r), the diameter (d) and the height (H).

The intriguing consequences of nanoengineering likewise work well in photoelectrochemical cell and lead to the exploitations in advanced nanoarchitecture that are extensively studied in bilateral classes.[41-44] This study deals with such burgeoning interests via putting forward two modern nanoarchitectures including the highly branched spikecubes exemplified by β-$SnWO_4$ and the biomimetic nanopeapods manifested in Au@Nb@$H_xK_{1-x}NbO_3$ for the first time to enrich the library of pattern designs for photoelectrocatalysis (Fig. 1.3).[45,46] In-depth discussions on these hierarchical structures begin with an argumentation on the interplay between the textural properties and the local chemical bonding between the constituent elements. The elaborations of the dependency of the architectural geometry on the coordination environment of these chemical systems and the synthetic methodologies follow up to gain a substantial insight into making and especially integrating the nanomaterials at a satisfactory precision level. All in all, this thesis

contributes to the synergism of overall atomic and nano-/micro-scopic treatments on the macroscopically photoelectrocatalytic activity.

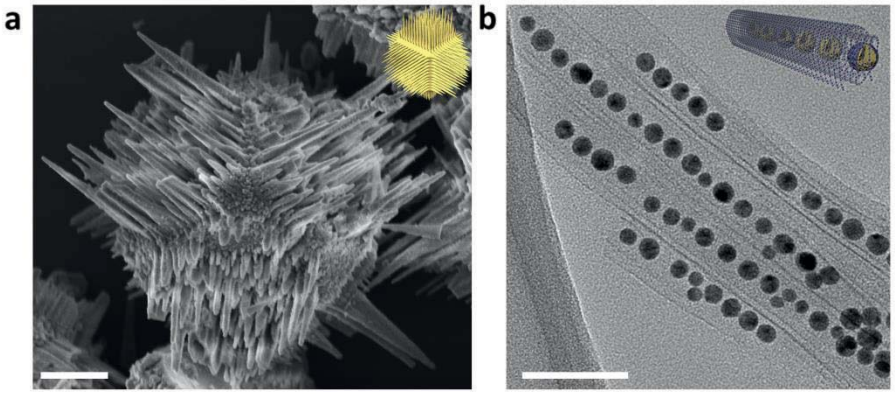

Figure 1. 3. (a) SEM image of multiarmed β-$SnWO_4$ spikecube (scale bar: 2 μm) and (b) TEM image of bioinspired Au@Nb@$H_xK_{1-x}NbO_3$ nanopeapods (scale bar: 50 nm) (*adapted from reference[45,46]*).

2. Principles of Heterogeneous Photoelectrocatalysis

In order to favor straightforward understanding of most discussions on the photoelectrocatalysis carried out by the topical β-$SnWO_4$ spikecubes and Au@Nb@$H_xK_{1-x}NbO_3$ nanopeapods artifacts throughout this dissertation, some fundamental nature and basic categories of photoelectrochemistry are first reviewed in this chapter.[33,34] The literal and schematic interpretations mostly deal with *n-type* semiconductors in terms of i) their popularity in the reported literature due to the better stability than that of *p-type* semiconductors and ii) the coincidence that both β-$SnWO_4$ and $H_xK_{1-x}NbO_3$ are *n-type* semiconductors.

2.1 Review of Energetics

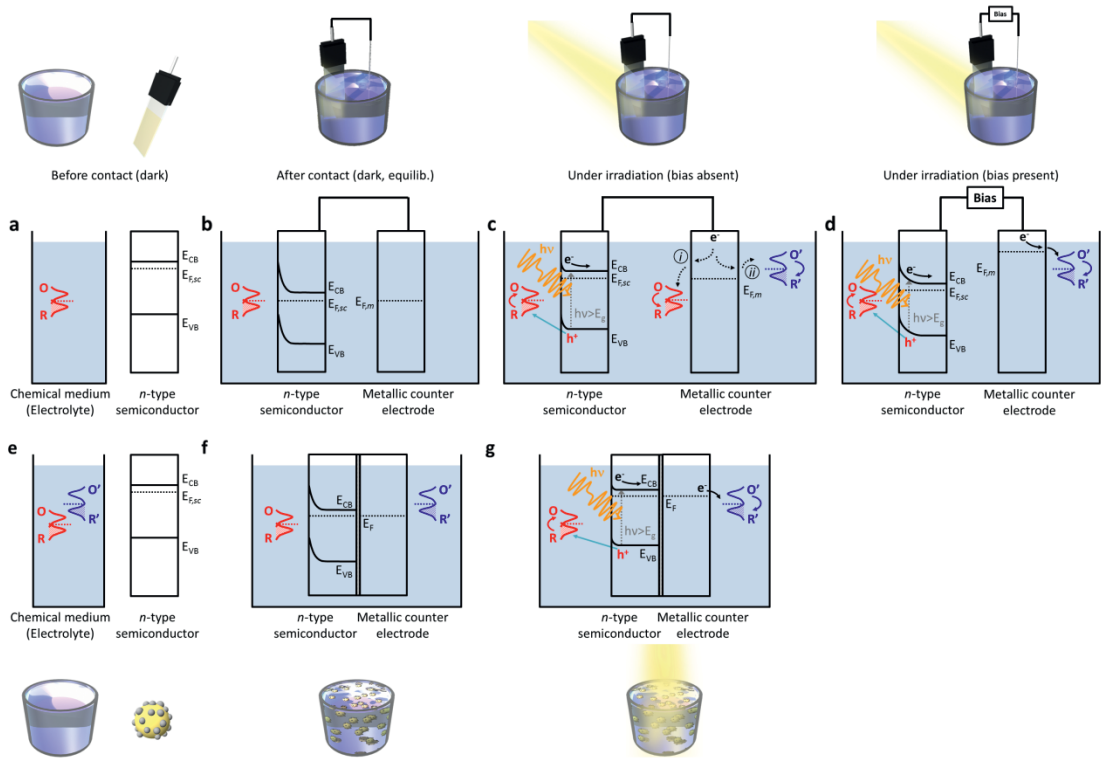

Figure 2. 1. Energetics evolutions in a (a-d) photoelectrochemical cell and (e-g) photochemical diode. (a,d) Energy diagrams of isolated solid and liquid constituents. (b,f) Formation of the semiconductor-electrolyte junction upon mutual contact. Effects of (c,g) suprabandgap light ($hv > E_g$) illumination and (d) electrical bias on the electronic structure of overall systems. Terms are defined in the text.

All phenomena associated with the "Becquerel effect" started exclusively with the formation of a semiconductor-electrolyte junction at a solid-liquid interface (Fig. 2.1). The semiconductor-electrolyte junction established in the presence of an initial difference in the Fermi

level (chemical potential of electrons) between these two phases. The Fermi level in the *n-type* semiconductor ($E_{F,sc}$) before contact with the electrolyte is located closely below the energy of the conduction band edge (E_{CB}). The Fermi level in the liquid phase is dictated by the presence of redox couples, and the energy is derived from the concentrations and standard potentials. Fig. 2.1a illustrates the conditions of a concurrent presence of the redox couple O and R

$$O + e^- \leftrightarrow R \tag{2.1}$$

in which the Fermi level is given by

$$E_{F,redox} = V^0_{redox} + k_B T \ln(\frac{[R]}{[O]}) \tag{2.2}$$

where $V°_{redox}$ (V vs. Normal Hydrogen Electrode (NHE)) is the standard redox potential of the redox couple O/R, k_B the Boltzmann constant, T (K) the absolute temperature and [R] and [O] are their concentrations (mol cm^{-3}), respectively. When the semiconductor is brought into contact with the electrolyte, charge transfer occurs at the boundary until the chemical potential of the electrons ($\overline{\mu_e}$) in the two phases are equivalent (Fermi level equalize). Fig. 2.1b depicts the conditions that the initial Fermi level in a *n-type* semiconductor is above that of the redox couple O/R in the solution, leading to an electron transfer from the semiconductor to the electrolyte. Upon the acceptance of the electron ($O + e^- \rightarrow R$), the electronic structure of the acceptor (O) changes, particularly, the unoccupied electronic state becomes occupied.

$$O + e^- \rightarrow O^- \tag{2.3}$$

The free energy change associated with this charge uptake step is a measure of the electron affinity (A) of O.

Given the polar nature of the liquid electrolyte, the dipoles in the solvent molecules coordinated to the redox species as a solvation sheath re-orientate in response to this charge variation.

$$O^- \rightarrow R \tag{2.4}$$

Such spontaneous relaxation of the solvation shell results in an additional energy release, the well-known solvent reorganization energy (λ_s). Values for λ_s can be few tenths of an electron volt (eV) up to 2 eV.[47] Moreover, thermal agitation of the solvation structure leads to a Gaussian distribution of the energy states ($D_o(E)$) for the redox species O,

$$D_O(E) = \exp[\frac{-(E - E_{F,redox} - \lambda_s)^2}{4\lambda_s kT}] \quad (2.5)$$

as depicted in Fig. 2.2. Herein, $E_{F,redox}$ (eV) described in terms of a Fermi distribution function corresponding to the energy state with a 50% probability of electron occupancy[47,48] for the redox couple O/R is

$$E_{F,redox} = -I + \lambda = -A - \lambda \quad (2.6)$$

I is the ionization potential of the coupled redox species R. Noteworthily, charge transfer occurs only at an overlap of the unoccupied redox states ($D_O(E)$) with occupied semiconductor states. In particular, $D_O(E)$ only becomes zero at energies of $E = \pm\infty$ and is at the maximum when $E = E_{F,redox} + \lambda_s$.

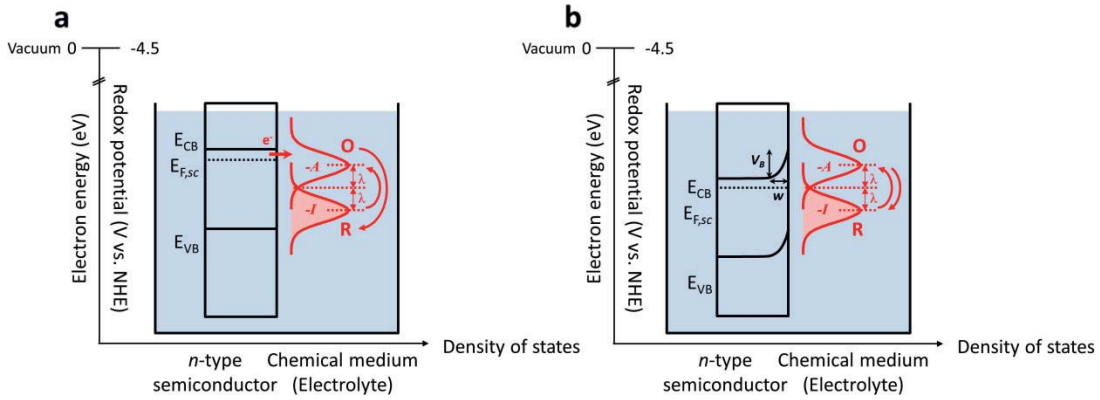

Figure 2. 2. (a) Energy diagram of an *n-type* semiconductor at the initial instant upon contact with the electrolyte with the redox couple O/R. The valence band, conduction band, and the Fermi level ($E_{F,SC}$) of the semiconductor and the distribution of the energy states for the redox species, the Fermi level ($E_{F,redox}$), λ_s, A of the electron acceptor O and the ionization potential (I) of the electron donor R are labeled alongside. Charge transfer carried out at the solid-liquid boundary and reaching (b) the electronic equilibrium at the established semiconductor-electrolyte junction. The developed depletion layer is characterized by the width (w) and the extent of the band bending (V_B).

This interfacial charge transfer results in a semiconductor that is positively charged in regard of the electrolyte. In particular, these charges exclusively distribute within a region adjacent to the interface with the electrolyte, which is designated as “space charge layer” (or “depletion layer” in terms of this space exhausted of majority charge carriers). As a consequence, an electric field is generated and expressed by the bending of the conduction and valence band edges in an upward direction. The extent of band bending (V_B) in the space charge layer is characterized by the difference between $E_{F,sc}$ and $V°_{redox}$. Specifically, the energy position of the Fermi level is

customarily expressed in units of eV with respect to vacuum (zero reference point) in solid state physics. In electrochemistry, the standard redox potential for redox couples is otherwise given in units of volt (V) with respect to NHE as the zero reference point corresponding to the standard redox potential of the proton-hydrogen (H^+/H_2) redox couple. The association between these scales has been corroborated by the effective work function (or Fermi level) of -4.5 eV with respect to vacuum for the standard H^+/H_2 redox couple at equilibrium[49] and is expressed as,

$$E_i\ (eV) = -4.5 - qV_i\ (V\ vs.\ NHE) \tag{2.7}$$

wherein q is the electronic charge. This upward band bending sets up a potential barrier particularly against excess electron transfer into the liquid phase, which is analogous to the rectifying function in the Schottky junction. The width of the depletion layer (w) is determined by,

$$w = \sqrt{2\varepsilon\varepsilon_0 V_B / qN_D} \tag{2.8}$$

wherein ε is the dielectric constant of the semiconductor, ε_0 the permittivity of free space, V_B (V) the degree of band bending, q the electronic charge and N_D (cm^{-3}) is the charge carrier density in the *n-type* semiconductor (equivalent to the density of donors). In typical cases w ranges from 10 nm to several micrometres.[34,47]

Concurrently, on the liquid side charged ions of opposite sign (negative in this case) adsorb onto the surface of the semiconductor for charge offset. In contrast to the semiconductor, the sorption of counter-ions develops only within the well-known Helmholtz double layer bearing a characteristic thickness of a few angstroms (Å) in terms of the carrier density in solution much higher than that in the semiconductor.[33,34,47,48,53] The presence of a Helmholtz layer is of special importance in terms of the electrolyte composition and responsible for the conduction and valence band edges of the semiconductor at the solid-liquid boundary (Fig. 2.3).[53] In other words, polarizing the semiconductor through an artificially applied bias (Fig. 2.1d) doesn't change the relative energy positions of band edges to that of the redox couple in the electrolyte. Such energetic dependency of the band edges exclusively on the chemistry at the phase boundary fairly mirrors another characteristic, namely the Fermi level pinning effect, in a Schottky junction.[34] Altogether, the junctions between semiconductor and liquid electrolytes are in many respects similar to a Schottky junction.

When suprabandgap light is casting at the semiconductor-electrolyte contact (Fig. 2.4), photons having energy hv, where h is the Planck constant and v is the frequency (Hz) of the incident photon, are absorbed by the semiconductor to create electron-hole pairs.

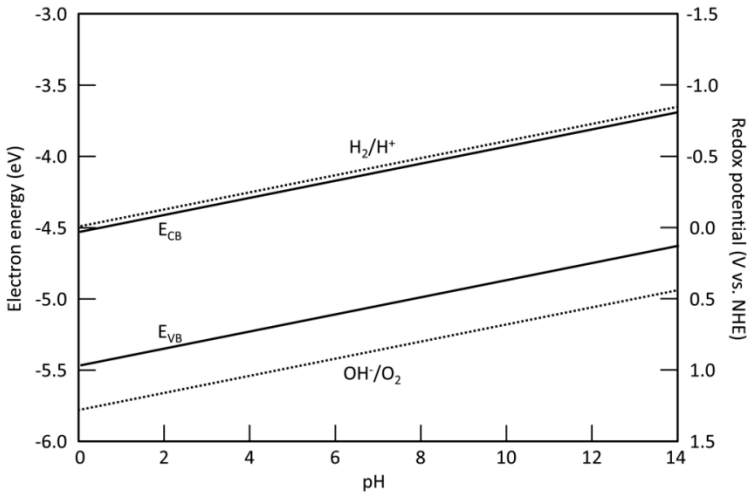

Figure 2. 3. Conduction and valence band edges of a semiconductor oxide plotted as a function of the pH value of coupled aqueous electrolyte. On the pH-E diagram, the E_{CB} and E_{VB} of a semiconductor linearly correlate to the pH value with a slope of 0.059 V/pH at 25 °C and 1 atm, lying alongside the thermodynamic limits of water electrolysis. This linear dependency is known as the Nernstian relation,[50-53] suggesting that in aqueous solutions H^+ and OH^- are the primary adsorbed species on the surface of a semiconductor within the Helmholtz layer.[50] Two energy scales (eV and V vs. NHE) are shown in parallel for comparison (*adapted from reference [47]*).

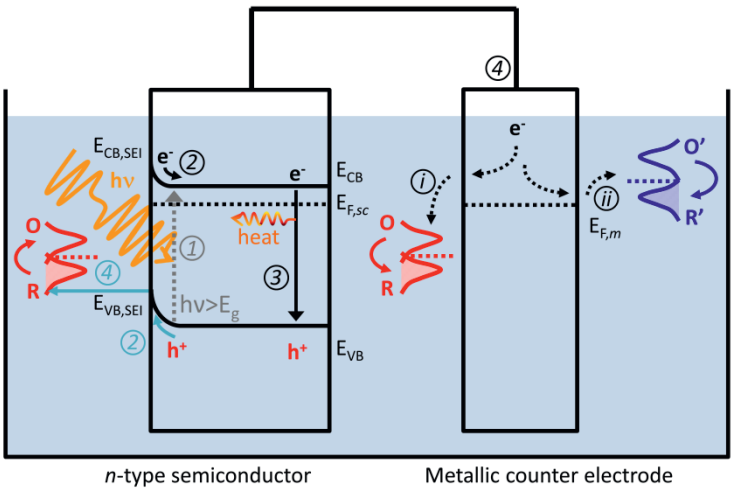

Figure 2. 4. Sequence of main processes in a photoelectrochemical cell, including charge generation upon suprabandgap light irradiation (1), subsequent individual charge transfer (2) or opposite-signed charges recombination (3) and eventual electrode/electrolyte interfacial redox reactions (4). The number of redox couples present in the electrolyte classifies the photoelectrochemical cell into (i) electrochemical photovoltaic cell and (ii) photoelectrocatalytic cell, respectively.

$$h\nu \rightarrow e_{SC}^{-} + h_{SC}^{+} \qquad (2.9)$$

The electron-hole pairs (excitons) of particular interest are those created in the depletion layer in terms of the built-in electric field resulting in their efficient separation, in which the electrons in the conduction band (CB) move towards the bulk of the *n-type* semiconductor while geminate holes in the valence band (VB) migrate to the solid-liquid phase boundary.

$$e^-_{depletionlayer} \rightarrow e^-_{bulk} \tag{2.10}$$

$$h^+_{depletionlayer} \rightarrow h^+_{semiconductor-liquid\ junction} \tag{2.11}$$

Most excitons photogenerated beyond the space charge layer suffer from recombination,

$$e^-_{bulk} + h^+_{bulk} \rightarrow heat\ (semicondcutor) \tag{2.12}$$

except for those that successfully escape from that process by virtue of the minority holes diffusion into the depletion layer. The photogeneration and subsequent separation of electron-hole pairs in the depletion layer brings about $E_{F,SC}$ arising to the pristine energy level (Fig. 2.1c), namely the energy position prior to the initialization of charge transfer at the semiconductor-electrolyte junction (Fig. 2.1a). This original energy status corresponds to a measure of the semiconductor potential with respect to NHE, wherein no excess charge is present in the semiconductor and which is designated as the "flatband" potential (V_{fb}). The holes effectively scavenged to the solid-liquid phase boundary react with redox specie R in the electrolyte at a potential corresponding to the band edge of VB at the semiconductor-electrolyte interface ($E_{V,SEI}$), leading to the oxidation of R to O.

$$h^+_{semiconductor-liquid\ junction} + R \rightarrow O \tag{2.13}$$

More or less, the charge carriers may trigger undesirable self-oxidation of the semiconductor depending on the thermodynamic redox potentials of the electrode decomposition reaction (Fig. 2.5).[33,54]

$$h^+_{semiconductor-liquid\ junction} + semiconductor \rightarrow oxidized\ semiconductor \tag{2.14}$$

Concurrently, the majority electrons delivered toward the semiconductor bulk are subsequently shuttled from the semiconductor *via* an external circuit to the metallic counter electrode and thereat injected into the electrolyte to drive a reduction reaction.

$$e^-_{bulk,SC} \rightarrow e^-_{bulk,m} \tag{2.15}$$

$$e^-_{bulk,m} + O \rightarrow R \tag{2.16}$$